Materials & Design 220 (2022) 110855

Contents lists available at ScienceDirect

Materials & Design

journal homepage: www.elsevier.com/locate/matdes

Tunable terahertz filter/antenna-sensor using graphene-based metamaterials

Meisam Esfandiyari [a], Ali Lalbakhsh [b,c,*], Saughar Jarchi [a], Mohsen Ghaffari-Miab [d], Hamideh Noori Mahtaj [e], Roy B.V.B. Simorangkir [f,*]

[a] Faculty of Technical and Engineering, Imam Khomeini International University, Qazvin, Iran
[b] School of Engineering, Macquarie University, Sydney, Australia
[c] School of Electrical and Data Engineering, University of Technology Sydney (UTS), Sydney, NSW 2007, Australia
[d] Faculty of Electrical and Computer Engineering, Tarbiat Modares University, Tehran, Iran
[e] Faculty of Electrical and Computer Engineering, Shahid Beheshti University, Tehran, Iran
[f] Tyndall National Institute, University College Cork, Dyke Parade, T12R5CP Cork, Ireland

HIGHLIGHTS

- A novel graphene integrated module for electromagnetic THz filtering, sensing and high-gain radiation patterns is proposed.
- The graphene-based metamaterial introduces an excellent tunability to the filters and the antennas in THz regime.
- The proposed module exhibits excellent performance for different wave polarizations and oblique incident angles.
- The maximum sensitivity of 0.145 THz/RIU is achieved for the proposed sensor.

GRAPHICAL ABSTRACT

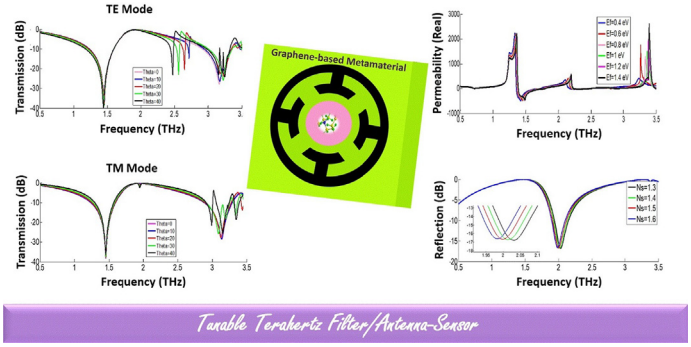

ARTICLE INFO

Article history:
Received 14 March 2022
Revised 13 June 2022
Accepted 13 June 2022
Available online 16 June 2022

Keywords:
Antenna-sensor
Dual band
Filter
Metamaterial
Multilayer graphene
Tunability

ABSTRACT

In this paper, a novel tunable graphene-based bandstop filter/antenna-sensor is presented. This structure is an integrated module that can be used to combine filtering and high-gain radiation performance. The initial design of the unit cell consists of four U-shaped stubs loaded, resembling the arms of a ring and a sensing layer in the substrate. The reflection and transmission spectra are obtained for various graphene's chemical potentials and refractive index of sensing layer (Ns) of structure in the range of 1.3–1.6 THz. The proposed structure exhibits the attributes of both dual-band filter and single-band antenna-sensor. The conductivity of graphene and its structural parameters are studied to optimize the component performance. In filtering mode, the first bandstop is from 1.23 to 1.6 THz equal to 26% of fractional bandwidth (FBW) at 1.415 THz. The second stopband is centered at 3.12 THz with FBW of 14% for Ns = 1.6 and 0.6 eV chemical potential. In the antenna mode, a single band of the antenna-sensor is centered at 1.95 THz for the same Ns and same chemical potential. It is shown that a sensitivity of 0.145 THz/RIU is achieved at Ns = 1.5 and chemical potential of 0.6 eV. Additionally, the performance of the proposed filter/antenna-sensor module is investigated for different wave polarizations and oblique angles.

* Corresponding authors at: School of Engineering, Macquarie University, Sydney, Australia (A. Lalbakhsh) and Tyndall National Institute, University College Cork, Dyke Parade, T12R5CP, Cork, Ireland (R. B. V. B. Simorangkir).
E-mail addresses: ali.lalbakhsh@mq.edu.au (A. Lalbakhsh), roy.simorangkir@tyndall.ie (R.B.V.B. Simorangkir).

https://doi.org/10.1016/j.matdes.2022.110855
0264-1275/

1. Introduction

Nowadays, there has been increasing attention to filter/antenna-sensors due to their simple configuration, multimodality sensing, passive operation, and low cost [1]. These new integrated structures introduced in this paper have three functionalities for communicating, sensing and filtering at once and will minimize the number of components and shrink the circuitry footprint. The purpose method of filter/antenna-sensors is established by their geometrical shape or their fundamental material of the structure and the alteration effect in terms of their antenna or filter resonance frequency, which is evaluated by these parameters influence on the reflection or transmission coefficient.

The principle of Surface Plasmon Resonance (SPR) and its application has been researched extensively in designing optical devices that are structured by metamaterials in the past decade [2–4]. Metamaterials are artificially-made structures possessing extraordinary electromagnetic properties that are not available in nature and have been used extensively in designing various types of filters, antennas and electromagnetic components [5–13]. Over the last decade, the combination of metamaterials and plasmonic has found its various applications, including SPR sensors [14,15], zero-index material and perfect lens [16], directivity enhancement of nano antennas [17] absorbers [18], modulators [19,20] and filters [21–27]. Recently, an increasing demand is observed for Terahertz (THz) broadband tunable filters [28,29], which are critical for modern and emerging applications, such as fiber-optic sensors, and wavelength-swept lasers, etc. It should be noted that there are other mature technologies for filter and antenna designs, such as microstrip technology [30–41] mostly associated with high loss at the THz regime. Tunable filter/antenna-sensors are good candidates for controlling transmitting waves due to their modularity, an essential attribute in sensing and communications.

There are two major methods for altering THz waves used in this paper. In the first method, materials properties and the action of physical deformation are changed. For example, resonant frequencies are dynamically controlled to offer the desired operating frequencies by driving the martensitic transformation [42]. Consequently, a dynamic band-stop filter range up to 0.56 THz was achieved.

In the second method, materials intrinsic features are used to adjust THz waves. Some materials in nature have varying permittivity or permeability based on external situations such as heat, electricity, magnetism, and light. Semiconductors or superconductors, phase change materials, ferroelectric or ferromagnetic materials, liquid crystal materials, and graphene are examples of these kinds of materials [43,44]. Among the materials listed, graphene has become a promising solution in recent years mainly because of its reconfigurability feature and produced using the micromechanical cleavage method since 2004 [44]. Graphene is a suitable material for plasmonic appliances in the THz frequency regime due to its meta-like properties. It is a one-atom-thick 2D system with excellent optical properties critical in many potential applications, thanks to its high carrier mobility and anomalous quantum Hall effect in electrical transport [45].

These days, there has been a lot of attention concentrated on tunable optical integrated modules to extend communication systems [46–48]. The advantages of such modules are simple configuration, multimodality sensing, passive operation, and the low cost of plasmonic integrated structure fabrication that are used for processing information [49–52]. Metal-based integrated structures display desired performance in the near-infrared region [53], but poor confinement of metal surface plasmon polariton (SPPs) in the THz range limits their application. In contrast, graphene SPPs have high field confinement in the THz range, hence graphene-based structures are a promising solution for tunable and reconfigurable integrated structures with superior performance. In detail, the carrier density in graphene can be electrically adjusted by a small bias voltage, leading to a fast tuning operation within a nanosecond, which makes graphene a suitable material for tunable filters/antennas-sensor [54,55]. Indeed, tuning (SPPs) enables graphene-based integrated structures tunability, including central frequency adjustability.

One of the modern methods of designing graphene-based components is based on artificial intelligence approaches, where an optimization algorithm is utilized to deliver an intuitive or non-intuitive configuration [56]. Different types of nature-based algorithms, such as particle swarm optimization [57,58], gray wolf optimization [59–61], various types of artificial neural networks [62–71], ant colony [72,73], and genetic algorithm [74] can be incorporated into designing procedures to minimize the computation cost of the design.

This paper introduces a new class of metamaterial-based filter/antennas-sensors. The proposed structure is composed of four U-shaped stubs and a sensing layer responsible for creating a dual bandstop response and a single band antenna. The operational mechanism of this proposed structure is discussed through its permeability (μ) and electric near field. The transmission and reflection spectra of these structures are analyzed through the variation of the graphene's chemical potential. Additionally, the sensitivity of the integrated structure is achieved by varying the refractive index of the sensing layer. In addition, the transmission and reflection spectra of the U-shaped stub structure are investigated for oblique angles of incidence for two polarizations.

2. Structure and simulation method

2.1. Graphene theory

In the THz band, the graphene conductivity σ_g is defined by the Kubo formula as $\sigma_g = \sigma_{intra} + \sigma_{inter}$[4]. At our investigated frequency regime (0.5 to 3.5 THz), σ_{inter} is insignificant and σ_{intra} is considered as graphene conductivity, as follows:

$$\sigma_{mono} = \sigma_{intra} = \frac{2e^2 K_B T}{\pi h^2} \cdot \frac{i}{w + i\tau^{-1}} [Ln(2\cosh(\frac{\mu_c}{K_B T}))]. \quad (1)$$

where e is the electron charge, K_B is Boltzmann's constant, T is the ambient temperature ($300\ K$) , $\hbar$ is the reduced Planck constant, τ is the relaxation time ($1ps$), ω is the angular frequency and μ_c is the chemical potential. In order to achieve a stronger resonance, twenty layers of graphene are used in the U-shaped stub loaded metamaterials, respectively. Multilayer graphene is essentially decoupled N-layers of graphene. thus, the conductivity of N-layer graphene is $N\sigma_{mono}(\omega)$ [75].

2.2. Calculating sensitivity

The resonance condition in the reflection or transmission spectra is accessible when the wave vector of decaying waves and the wave vector of surface plasmons are equal, that this event leading to the creation of surface plasmon polaritons. However, this generation requires a prism, a grating and a defect on the metal surface or an optical fiber. Generally, angle and wavelength methods are two approaches for analyzing and investigating plasmonic sensors. Sensitivity (S) is the main factor for defining the performance of a sensor that is expressed by: $S = \frac{\sigma f_{res}}{\sigma N_s}$. If the refractive index of the sensing layer differs by σN_s, the frequency of the sensor differs by σf_{res} in the reflection or in the transmission spectra.

2.3. U-shaped stub metamaterial unit cell

A tunable, dual-band stopband filter and a tunable single-band antenna composed of four U-shaped stubs resembling the arms of a ring unit cell is designed and shown in Fig. 1. Each U-shaped stub of the ring operates as a high-low impedance transmission line equivalent to a series LC resonator. The application of these U-shaped stub results in a compact size of structure and a controllable harmonic frequency response, not possible using the basic circular ring. A nanofluidic channel as a sensing layer is created in the substrate of the unit cell. Each layer of the unit cell microstructure is located at a distance h from the underneath layer which includes SiO_2 film with permittivity of 3.9.

Geometrical dimensions of the U-stub metamaterial are: $R = 50\mu m$, $r = 40\mu m$, $R1 = 20\mu m$, $R2 = 30\mu m$,$p = 60\mu m$, $h = 7.5\mu m$, $g = 8\mu m$,$Rs = 8\mu m$.

3. Results and discussion

In this section, we first examine the filter/antenna properties and then the sensor properties will be investigated.

3.1. Filter/Antenna application

Recently, various computational approaches, such as finite element, finite difference time domain, Finite-difference frequency-domain have been used for computing parameters of microwave and optical components including photonic crystals [76–86], various types of filters [87–91], and electromagnetic devices [92–94]. In this paper, we used CST Microwave Studio (CST MWS) software for predicting all outputs if the proposed structure. In detail, the periodic boundary condition of CST MWS was used to numerically predict all consequences of the proposed component. Here, transmission and reflection spectra of the structure are investigated where a normal incidence THz wave is illuminated. In this section the refractive index of the sensing layer considers to be a constant equal 1.6 and the properties of the filter/antenna are investigated for various chemical potential. As illustrated in Fig. 2 b, the reflection spectrum is simulated and plotted for the proposed filter/antenna device and for different chemical potentials of 0.4, 0.6, 0.8, 1, 1.2 and 1.4 eV. As observed in the results, reflection spectrum exhibits a single resonance at 1.89, 1.95, 1.96, 1.98, 2 and 2.03 THz, respectively. Moreover, as the resonance frequency increases, the corresponding depth increases, highlighting the adjustability of the proposed structure and its sensing ability simultaneously.

The transmission spectrum exhibits two dips at 1.415 and 3.12 THz with bandwidths of 0.37and 0.42 THz and with $\mu_c = 0.6eV$ and Ns = 1.6 for a single layer of the U-stub metamaterial, where larger values of the chemical potential result in resonances at higher frequencies, as shown in Fig. 2 c. The quality factor is the ratio of resonance frequency to bandwidth as $Q = \frac{f_r}{B} = \frac{\sqrt{LC}}{\frac{R}{L}} = \frac{W_0}{\frac{R}{L}}$. Consequently, an equation for the RLC circuit can be written as: $B = \frac{R}{L} = \frac{W_0}{Q}$, and the bandwidth can be obtained as BW= R_{eff}/L, where L is the inductance and R_{eff} is the effective electrical resistance [95]. As a result, the strengthened coupling resistance increases, which in turn widens the bandwidth of the stopband filter. The filter bandwidth has a direct relationship with the effective electrical resistance.

Additionally, real permeability (μ) of the unit cell is obtained to further explore the characteristics of the filter/antenna for different shapes of loop resonators. It is worth noting that μ is derived from S-parameters [96]. As illustrated in Fig. 2 a, the negative-permeability of the unit cell induced negative group delay to cancel the coupling currents, which causes device acts as a bandstop filter. When permeability changes from a negative to positive amount, it would cross zero, and a single band reflection occurs.

Regarding the antenna properties, radiation pattern of the antenna is obtained where the chemical potential is set to 0.6 eV and the refractive index is considered 1.6 and 1.3, as illustrated in Fig. 3 a and b. The obtained gains are 14.9 and 15 dB at the resonant frequencies of 1.95 and 2 THz for Ns = 1.3 and 1.6.

The obtained gains for other chemical potential of 0.4, 0.8 and 1 eV are 14.5, 15.1 and 15.2 dB at their resonance frequencies and Ns = 1.6, respectively.

Regarding the filter properties and the better understand of bandstop filter mechanism, the electric field distribution throughout the U-shaped stub is investigated. The effective refractive index for the graphene plasmon (GPs) is $n_{eff} = \beta/k_0$ [4], where β is the propagation constant of the GPs and k_0 is the free space wavenumber. According to the Fabry-Perot (F-P) model, the resonant wavelength is $\lambda_{eff} = \frac{n_{eff} l_{eff}}{m + \frac{\varphi}{2\pi}}$, where l_{eff} is the effective F-P cavity length and φ is the phase shift of GPs and m can be regarded as the order of resonance [28,29].

As illustrated in Fig. 4, at frequencies which the n_{eff} is small, the resonance modes of the two adjacent unit cells in u-shaped stub are strongly coupled, while the resonance exposes an inward cou-

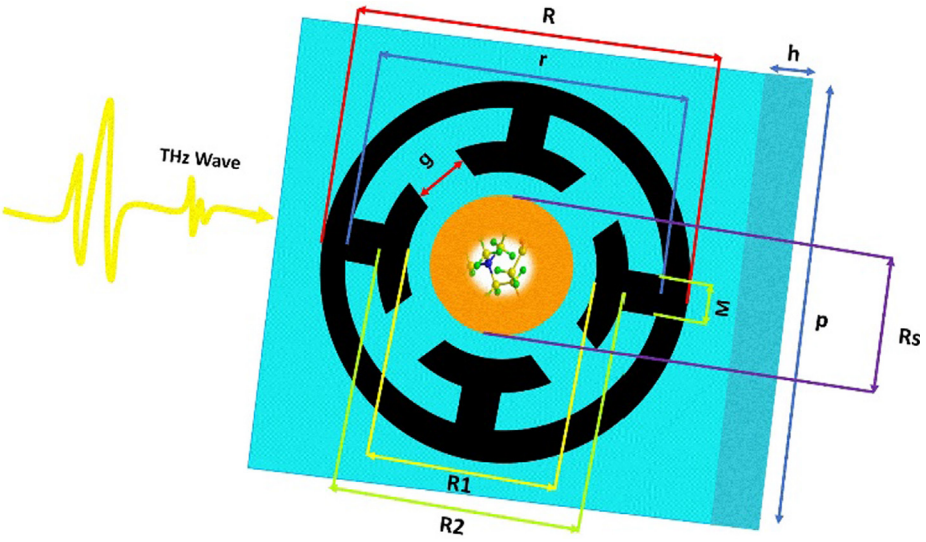

Fig. 1. Configuration of the single-layer U-shaped stub loaded metamaterial.

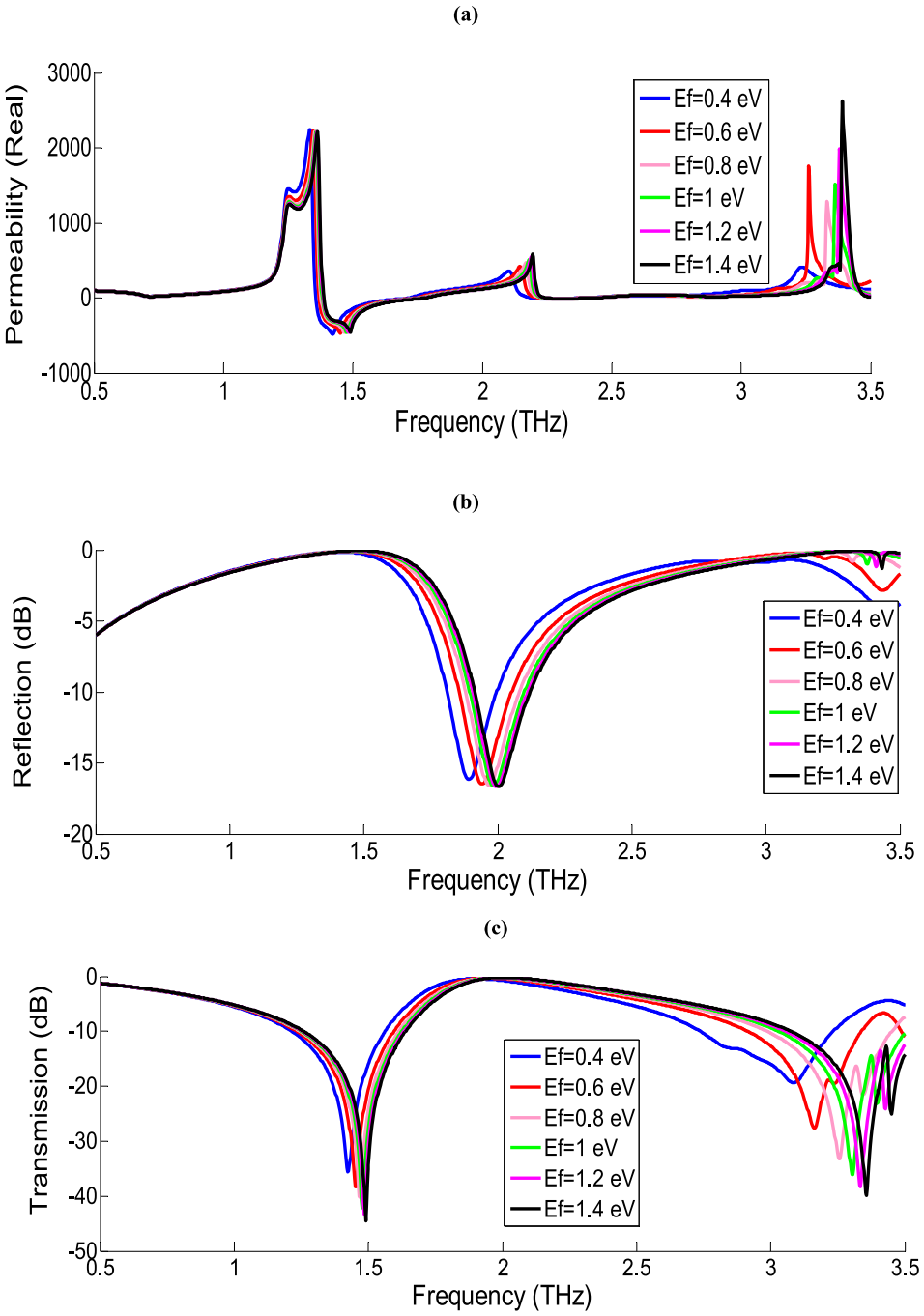

Fig. 2. **(a)** Real permeability of Configuration of the single-layer U-shaped stub loaded metamaterial. **(b)** reflection and **(c)** transmission spectra for the U-shaped stub loaded metamaterial and for four different chemical potentials of 0.4, 0.6, 0.8 and 1 eV.

pling at the corresponding frequency of the decreasing edge of the refractive index curve, i.e., 1.9 THz (Fig. 4). At the center frequency of stopband, i.e. f = 1.4 THz, where the n_{eff} is high, the resonance mode for the electric near-field exhibits the plasmonic hybridization [97]. In this paper similar results for the second resonance frequency of U-shaped stub metamaterial at three frequencies of 2.8, 3.3, and 3.5 THz as illustrated in Fig. 4, are obtained.

In what follows, the reflection and transmission spectra of the U-shaped stub array for chemical potential of 0.6 eV when Ns = 1.6 and various polarizations and also incidence angles are investigated. Due to the structure symmetry, the reflection and transmission resonances of the introduced filter/antenna-sensor is non-sensitive to the polarization of incoming waves for TE polarization as shown in Fig. 5a and b.

As the incident angle (TE polarization) increases, the first resonance of the stopband and the antenna resonance and their corresponding bandwidth remain almost unchanged for grades up to 40°, as shown in Fig. 5c-d. However, the second band is more sensitive to the incident angle and represents the same rejection band for incident angles up to 10° for the TE- polarization.

When an electromagnetic wave excites the structure, four stubs of the split-ring structure support in-phase current oscillations, except in a narrow frequency range in which an antisymmetric current is established and the E-field becomes parallel to the Z-

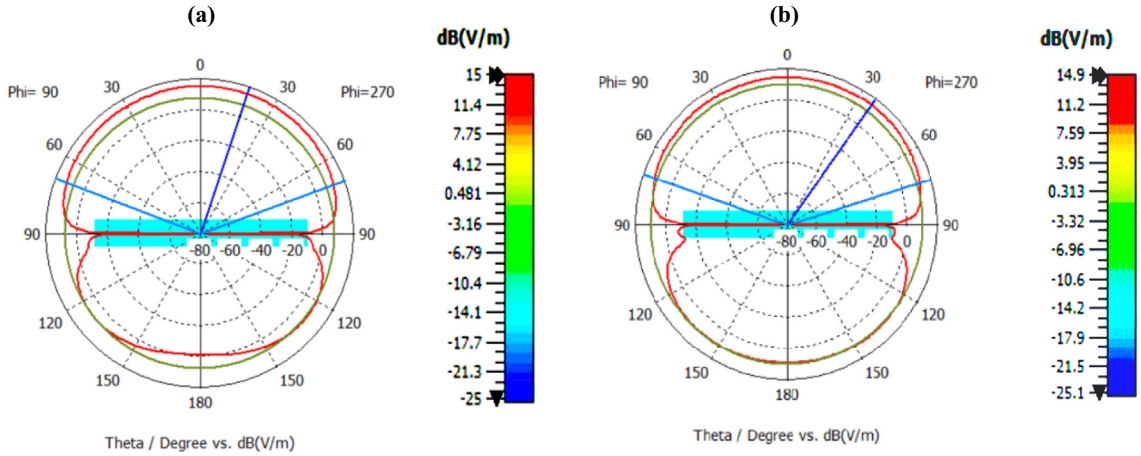

Fig. 3. The radiation patterns of the filter/antenna-sensor. (a) at the resonant frequency of 2 THz and Ns = 1.3 with chemical potential of 0.6 eV. (b) at the resonant frequency of 1.95 THz and Ns = 1.6 with chemical potential of 0.6 eV.

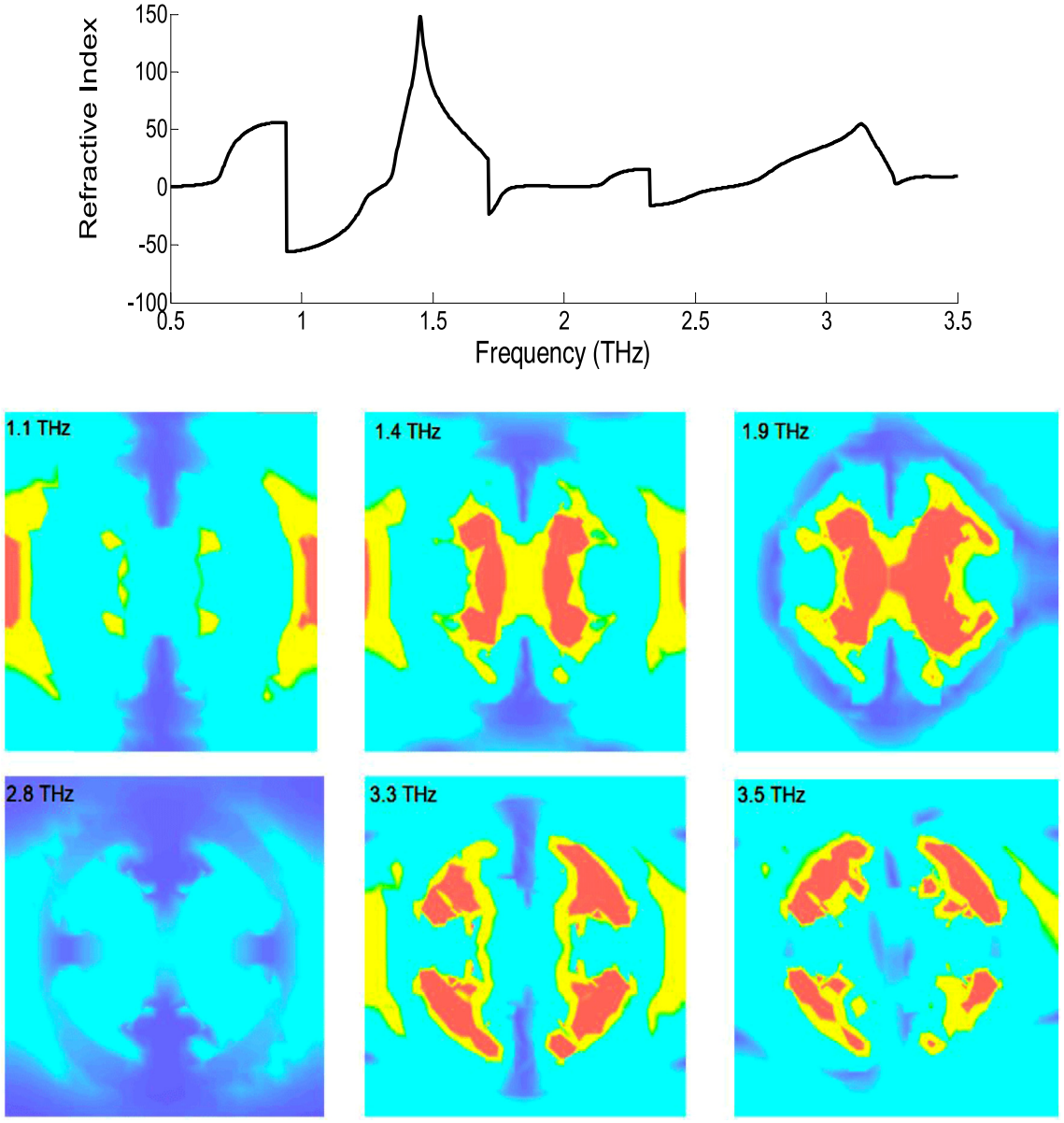

Fig. 4. Effective refractive index of the U-shaped stub loaded metamaterial at chemical potential of 0.6 eV and Ns = 1.6 and simulated magnitudes of electric near-fields in the top layer of the unit cell at frequencies of 1.1, 1.4, 1.6, 2.8, 3.3 and 3.5 THz, respectively.

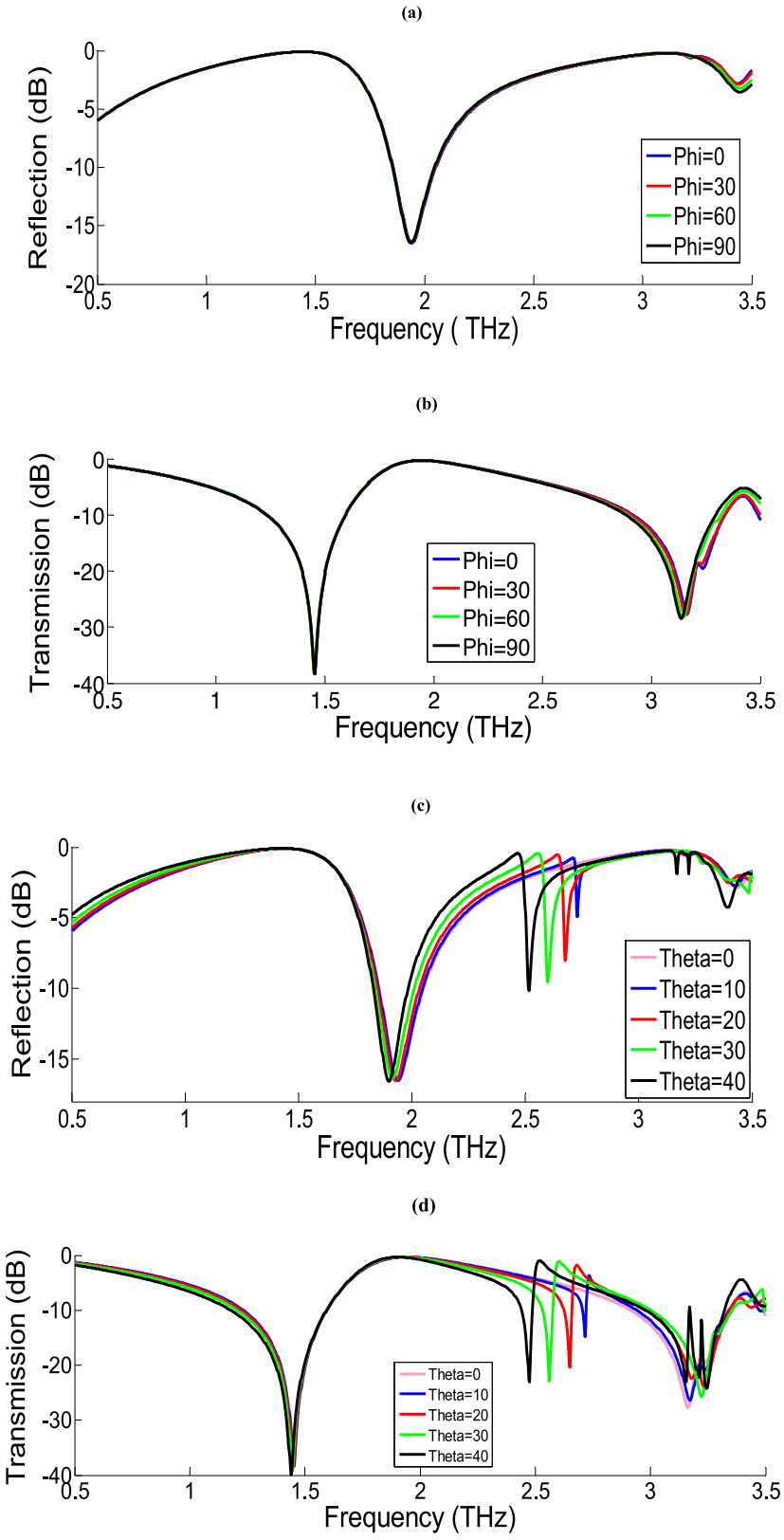

Fig. 5. **(a)** Reflection and **(b)** transmission curve as a function of polarization angle (phi) **(c)** reflection and **(d)** transmission curves as a function of oblique incidence at chemical potential of 0.6 eV and Ns = 1.6 for TE polarization.

axis. This condition leads to the excitation of a sharp asymmetric line-shaped Fano resonance which can be seen in Fig. 5c and d. As it is shown, the depth of the Fano resonance increases with the increase of theta.

In addition, for the chemical potential of 0.6 eV and Ns = 1.6, the U-shaped stub array reflection and transmission spectra are non-sensitive under the polarization of incoming waves for TM polarization, as shown in Fig. 5a and b.

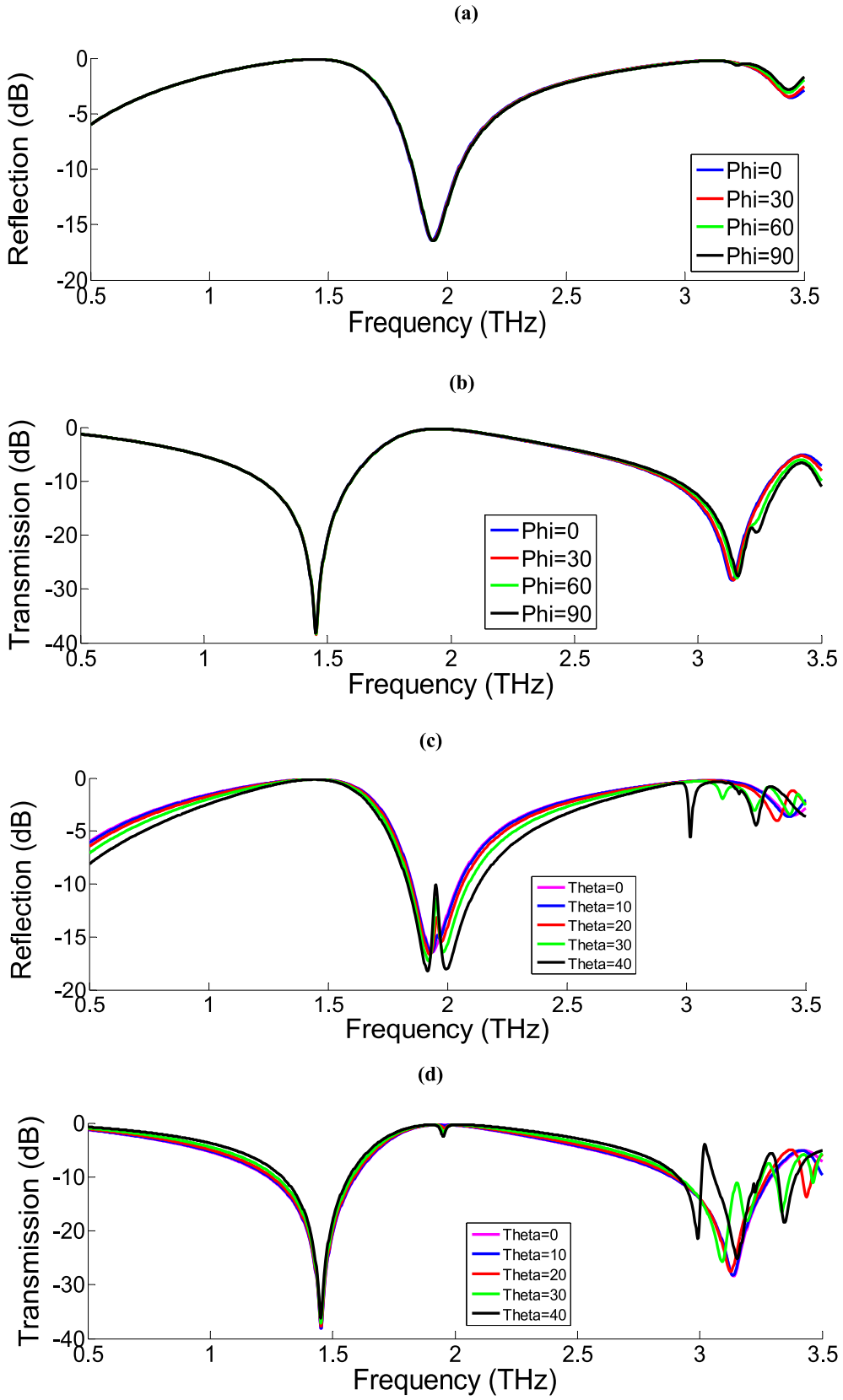

Fig. 6. **(a)** Reflection and **(b)** transmission curve as a function of polarization angle (phi) **(c)** reflection and **(d)** transmission curves as a function of oblique incidence at chemical potential of 0.6 eV and Ns = 1.6 for Tm polarization.

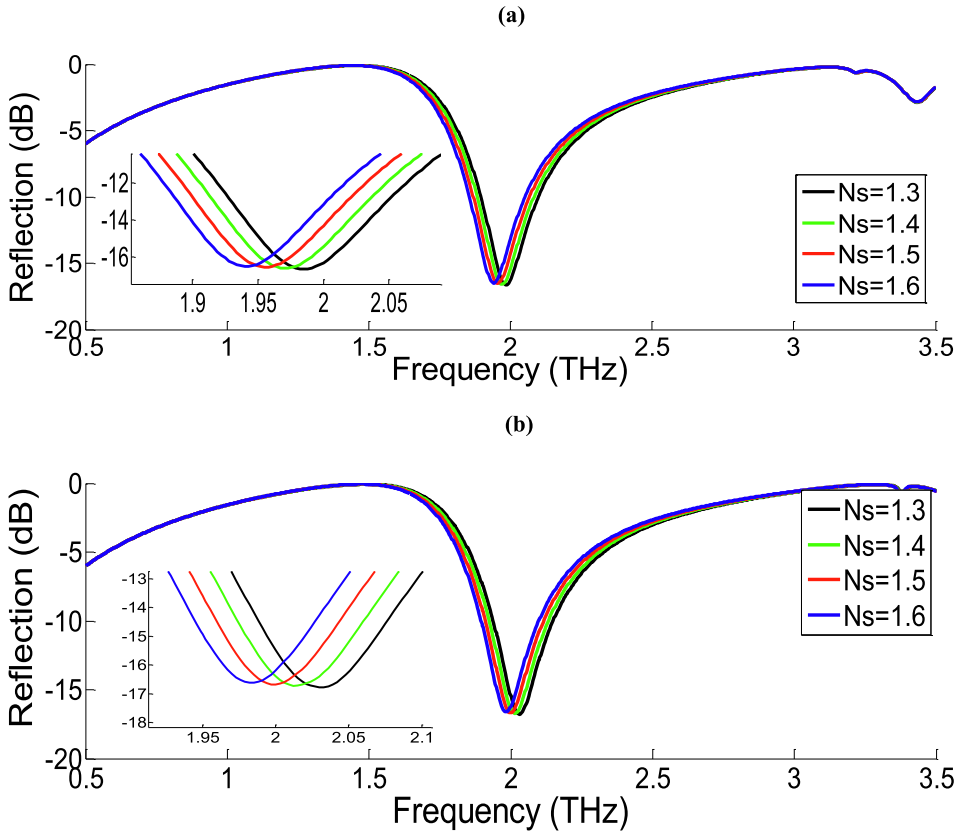

Fig. 7. Reflection of the filter/antenna-sensor as a function of refractive index of the sensing layer and (a) chemical potential of 0.6 eV and (b) 1 eV.

However, regarding the incident angle (TM polarization), the first resonance of the stopband filter and its corresponding bandwidth remains nearly unchanged for grades up to 40°. However, the second band is more sensitive to the incident angle and represents the same rejection band for incident angles up to 10° for the TM- polarization. The resonance frequency of the antenna is also non-sensitive up to 20° for TM- polarization (see Fig. 6).

3.2. Sensor application

In this section, the sensitivity of the structure is investigated. The scattering parameter [S11] of the filter/antenna-sensor defines the electrical performance of the sensor. It is calculated and studied with changing the refractive index of the sensing layer (Ns) in the range of 1.3 to 1.6 and is shown in Fig. 7a and 7b. As shown in Fig. 7, the resonance frequency of the sensor, when the wave is reflected from the structure, decreases with increasing refractive index of the sensing layer. It is observed that sensitivity is 0.145 THz/RIU and 0.17 THz/RIU at Ns = 1.5 when $\mu_c = 0.6$ and 1 eV respectively.

4. Conclusion

In this article, a tunable, dual bandstop filter and a single-band antenna-senor is designed and simulated in the THz regime. The central frequency of the filter and antenna-sensor is tuned by varying graphene chemical potential. The depth of reinforced resonances of the structure can be improved by increasing the number of graphene layers. The reinforced resonances in an interval approximately frequencies of 0.01, 0.3 and 0.1 THz can be covered when the chemical potential is varied between 0.4 and 1 eV in the first and second band of the filter and the single band antenna, respectively. Additionally, a sensitivity of 0.145 THz/RIU is achieved at Ns = 1.5 and in chemical potential of 0.6 eV.

Declaration of Competing Interest

The authors declare that they have no known competing financial interests or personal relationships that could have appeared to influence the work reported in this paper.

References

[1] H. Huang, Flexible Wireless Antenna Sensor: A Review, IEEE Sensors J. 13 (10) (2013) 3865–3872.
[2] M. Esfandiari, S. Jarchi, P. Nasiri-Shehni, M. Ghaffari-Miab, Enhancing the sensitivity of a transmissive graphene-based plasmonic biosensor, Appl. Opt. 60 (5) (2021) 1201–1208.
[3] D.K. Gramotnev, S.I. Bozhevolnyi, Plasmonics beyond the diffraction limit, Nat. Photonics 4 (2) (2010) 83–91.
[4] A. Vakil, Transformation Optics using Graphene: One-atom-thick Optical Devices Based on Graphene, University of Pennsylvania, 2012.
[5] A. Iqbal et al., Electromagnetic bandgap backed millimeter-wave MIMO antenna for wearable applications, IEEE Access 7 (2019) 111135–111144.
[6] A. Lalbakhsh, M.U. Afzal, K.P. Esselle, S.L. Smith, All-Metal Wideband Frequency-Selective Surface Bandpass Filter for TE and TM polarizations, IEEE Trans. Antennas Propag. 70 (4) (2022) 2790–2800.
[7] M.U. Afzal, K.P. Esselle, A. Lalbakhsh, A Methodology to Design A Low-Profile Composite-Dielectric Phase-Correcting Structure, IEEE Antennas Wireless Propag. Lett. 17 (7) (2018) 1223–1227.
[8] A. Iqbal, A. Bouazizi, O.A. Saraereh, A. Basir, R.K. Gangwar, Design of multiple band, meandered strips connected patch antenna, Prog. Electromagn. Res. Lett. 79 (2018) 51–57.
[9] A. Lalbakhsh, M.U. Afzal, T. Hayat, K.P. Esselle, K. Mandal, All-metal wideband metasurface for near-field transformation of medium-to-high gain electromagnetic sources, Sci. Rep. 11 (1) (2021). pp. 1–9-1–9.
[10] A. Goudarzi, M.M. Honari, R. Mirzavand, Resonant cavity antennas for 5G communication systems: a review, Electronics 9 (7) (2020) 1080.
[11] M. Zandvakili, M.M. Honari, P. Mousavi, D. Sameoto, Gecko-Gaskets for Multilayer, Complex, and Stretchable Liquid Metal Microwave Circuits and Antennas, Adv. Mater. Technol. 2 (11) (2017) 1700144.
[12] H. Saghlatoon, R. Mirzavand, M.M. Honari, P. Mousavi, Sensor antenna transmitter system for material detection in wireless-sensor-node applications, IEEE Sens. J. 18 (21) (2018) 8812–8819.
[13] A. Lalbakhsh, R.B. Simorangkir, N. Bayat-Makou, A.A. Kishk, K.P. Esselle, Advancements and artificial intelligence approaches in antennas for

environmental sensing, in: Artificial Intelligence and Data Science in Environmental Sensing, 2022, pp. 19–38.
[14] M. Esfandiyari, M. Norouzi, P. Haghdoust, S. Jarchi, Study of a surface plasmon resonance optical fiber sensor based on periodically grating and graphene, Silicon 10 (6) (2018) 2711–2716.
[15] A. Upadhyay, Y. Prajapati, V. Singh, J. Saini, Comprehensive study of reverse index waveguide based sensor with metamaterial as a guiding layer, Opt. Commun. 348 (2015) 71–76.
[16] J.B. Pendry, Negative refraction makes a perfect lens, Phys. Rev. Lett. 85 (18) (2000) 3966–3969.
[17] M. Esfandiyari, S. Jarchi, M. Ghaffari-Miab, Channel capacity enhancement by adjustable graphene-based MIMO antenna in THz band, Opt. Quant. Electron. 51 (5) (2019) 1–11.
[18] J. Grant, Y. Ma, S. Saha, L. Lok, A. Khalid, D. Cumming, Polarization insensitive terahertz metamaterial absorber, Opt. Lett. 36 (8) (2011) 1524–1526.
[19] S. He, X. Zhang, Y. He, Graphene nano-ribbon waveguides of record-small mode area and ultra-high effective refractive indices for future VLSI, Opt. Express 21 (25) (2013) 30664–30673.
[20] L. Ju, B. Geng, J. Horng, C. Girit, M. Martin, Z. Hao, H.A. Bechtel, X. Liang, A. Zettl, Y.R. Shen, F. Wang, Graphene plasmonics for tunable terahertz metamaterials, Nat. Nanotechnol. 6 (10) (2011) 630–634.
[21] N. Han, Z. Chen, C. Lim, B. Ng, M. Hong, Broadband multi-layer terahertz metamaterials fabrication and characterization on flexible substrates, Opt. Express 19 (8) (2011) 6990–6998.
[22] X. Li, L. Yang, C. Hu, X. Luo, M. Hong, Tunable bandwidth of band-stop filter by metamaterial cell coupling in optical frequency, Opt. Express 19 (6) (2011) 5283–5289.
[23] Z. Li, G. Sun, P. Zhao, Y. J. Ding, Q. Gan, Instantaneous release of broadband terahertz radiation trapped by periodic arrays of split-ring resonators, in: 2012 Conference on Lasers and Electro-Optics (CLEO), 2012, IEEE, pp. 1–2.
[24] C. Zhang et al., Graphene-based anisotropic polarization meta-filter, Mater. Des. 206 (2021) 109768.
[25] M. Rodner, J. Bahonjic, M. Mathisen, R. Gunnarsson, S. Ekeroth, U. Helmersson, I.G. Ivanov, R. Yakimova, J. Eriksson, Performance tuning of gas sensors based on epitaxial graphene on silicon carbide, Mater. Des. 153 (2018) 153–158.
[26] S. Venkatachalam, G. Ducournau, J.-F. Lampin, D. Hourlier, Net-shaped pyramidal carbon-based ceramic materials designed for terahertz absorbers, Mater. Des. 120 (2017) 1–9.
[27] J. Gong, H. Tang, M. Wang, X. Lin, K. Wang, J. Liu, Novel three-dimensional graphene nanomesh prepared by facile electro-etching for improved electroanalytical performance for small biomolecules, Mater. Des. 215 (2022) 110506.
[28] Y. Gao, G. Ren, B. Zhu, L. Huang, H. Li, B. Yin, S. Jian, Tunable plasmonic filter based on graphene split-ring, Plasmonics 11 (1) (2016) 291–296.
[29] B. Shi, W. Cai, X. Zhang, Y. Xiang, Y.u. Zhan, J. Geng, M. Ren, J. Xu, Tunable band-stop filters for graphene plasmons based on periodically modulated graphene, Sci. Rep. 6 (1) (2016).
[30] H. Heshmati, S. Roshani, A miniaturized lowpass bandpass diplexer with high isolation, AEU-Int. J. Electron. Commun. 87 (2018) 87–94.
[31] A. Pirasteh, S. Roshani, S. Roshani, A modified class-F power amplifier with miniaturized harmonic control circuit, AEU-Int. J. Electron. Commun. 97 (2018) 202–209.
[32] S. Roshani, K. Dehghani, S. Roshani, A Lowpass Filter Design Using Curved and Fountain Shaped Resonators, Frequenz 73 (7–8) (2019) 267–272.
[33] M. Hookari et al., High-efficiency balanced power amplifier using miniaturized harmonics suppressed coupler, Int. J. RF Microwave Comput. Aided Eng. 30 (8) (2020) e22252.
[34] S. Lotfi et al., Design of a miniaturized planar microstrip Wilkinson power divider with harmonic cancellation, Turkish J. Electr. Eng. Comput. Sci. 28 (6) (2020) 3126–3136.
[35] A. Pirasteh, S. Roshani, S. Roshani, Design of a miniaturized class F power amplifier using capacitor loaded transmission lines, Frequenz 74 (3-4) (2020) 145–152.
[36] S.K. Bavandpour et al., A compact lowpass-dual bandpass diplexer with high output ports isolation, AEU-Int. J. Electron. Commun. 135 (2021) 153748.
[37] S. Roshani, S. Roshani, A compact coupler design using meandered line compact microstrip resonant cell (MLCMRC) and bended lines, Wireless Netw. 27 (1) (2021) 677–684.
[38] A. Lalbakhsh et al., Design of a compact planar transmission line for miniaturized rat-race coupler with harmonics suppression, IEEE Access 9 (2021) 129207–129217.
[39] G. Karimi et al., Design of modified Z-shaped and T-shaped microstrip filter based on transfer function analysis, Wireless Personal Commun. 82 (4) (2015). 2005–2016-2005–2016.
[40] A. Lalbakhsh, M.U. Afzal, K.P. Esselle, S.L. Smith, A High-gain Wideband EBG Resonator Antenna for 60 GHz Unlicenced Frequency Band, in: 12th European Conference on Antennas and Propagation (EuCAP 2018).
[41] K. Dehghani, G. Karimi, A. Lalbakhsh, S.V. Maki, Design of lowpass filter using novel stepped impedance resonator, Electron. Lett. 50 (1) (2014) 37–39.
[42] L.G. Melo, Theory of magnetically controlled low-terahertz surface plasmon-polariton modes in graphene–dielectric structures, JOSA B 32 (12) (2015) 2467–2477.
[43] C.H. Gan, H.S. Chu, E.P. Li, Synthesis of highly confined surface plasmon modes with doped graphene sheets in the midinfrared and terahertz frequencies, Phys. Rev. B 85 (12) (2012) 125431.
[44] M. Jablan, H. Buljan, M. Soljačić, Plasmonics in graphene at infrared frequencies, Phys. Rev. B 80 (24) (2009) 245435.
[45] K.S. Novoselov et al., Two-dimensional gas of massless Dirac fermions in graphene, Nature 438 (7065) (2005) 197–200.
[46] X. He, F. Liu, F. Lin, W. Shi, Tunable terahertz Dirac semimetal metamaterials, J. Phys. D Appl. Phys. 54 (23) (2021) 235103.
[47] J. Leng et al., Investigation of terahertz high Q-factor of all-dielectric metamaterials, Opt. Laser Technol. 146 (2022) 107570.
[48] X. He, F. Lin, F. Liu, W. Shi, Tunable terahertz Dirac-semimetal hybrid plasmonic waveguides, Optical Mater. Exp. 12 (1) (2022) 73–84.
[49] K.S. Novoselov, A. Geim, The rise of graphene, Nat. Mater. 6 (3) (2007) 183–191.
[50] M.S. Khan, G. Varshney, P. Giri, Altering the multimodal resonance in ultrathin silicon ring for tunable THz biosensing, IEEE Trans. Nanobiosci. 20 (4) (2021) 488–496.
[51] G. Varshney, P. Giri, Bipolar charge trapping for absorption enhancement in a graphene-based ultrathin dual-band terahertz biosensor, Nanoscale Adv. 3 (20) (2021) 5813–5822.
[52] G. Varshney, S. Gotra, V. Pandey, R. Yaduvanshi, Proximity-coupled graphene-patch-based tunable single-/dual-band notch filter for THz applications, J. Electron. Mater. 48 (8) (2019) 4818–4829.
[53] F. Bonaccorso, Z. Sun, T. Hasan, A. Ferrari, Graphene photonics and optoelectronics, Nat. Photonics 4 (9) (2010) 611–622.
[54] S.R. Mirnaziry, A. Setayesh, M.S. Abrishamian, Design and analysis of plasmonic filters based on stubs, JOSA B 28 (5) (2011) 1300–1307.
[55] A. Setayesh, S.R. Mirnaziry, M.S. Abrishamian, Numerical investigation of tunable band-pass\band-stop plasmonic filters with hollow-core circular ring resonator, J. Opt. Soc. Korea 15 (1) (2011) 82–89.
[56] H.M. Nemat-Abad, E. Zareian-Jahromi, R. Basiri, Design of Metasurface-Based Multi-layer THz Filters Utilizing Optimization Algorithm with Distinct Fitness Function Definitions, Plasmonics 16 (5) (2021) 1865–1876.
[57] A. Lalbakhsh, M.U. Afzal, K.P. Esselle, Multi-objective Particle Swarm Optimization to Design a Time Delay Equalizer Metasurface for an Electromagnetic Band Gap Resonator Antenna, IEEE Antennas Wireless Propag. Lett. 16 (2017) 912–915.
[58] A. Lalbakhsh, M.U. Afzal, K.P. Esselle, S. Smith, Design of an artificial magnetic conductor surface using an evolutionary algorithm, in: Proc. Int. Conf. Electromagnetics in Advanced Applications (ICEAA), 2017, pp. 885–887-885–887.
[59] M. Roshani et al., Evaluation of flow pattern recognition and void fraction measurement in two phase flow independent of oil pipeline's scale layer thickness, Alexandria Eng. J. 60 (1) (2021) 1955–1966.
[60] A. Karami, G.H. Roshani, E. Nazemi, S. Roshani, Enhancing the performance of a dual-energy gamma ray based three-phase flow meter with the help of grey wolf optimization algorithm, Flow Meas. Instrum. 64 (2018) 164–172.
[61] E. Nazemi et al., Optimization of a method for identifying the flow regime and measuring void fraction in a broad beam gamma-ray attenuation technique, Int. J. Hydrogen Energy 41 (18) (2016) 7438–7444.
[62] M.A. Sattari, G.H. Roshani, R. Hanus, E. Nazemi, Applicability of time-domain feature extraction methods and artificial intelligence in two-phase flow meters based on gamma-ray absorption technique, Measurement 168 (2021) 108474.
[63] M. Roshani et al., Combination of X-ray tube and GMDH neural network as a nondestructive and potential technique for measuring characteristics of gas-oil–water three phase flows, Measurement 168 (2021).
[64] M. Roshani et al., Proposing a gamma radiation based intelligent system for simultaneous analyzing and detecting type and amount of petroleum by-products, Nucl. Eng. Technol. 53 (4) (2021) 1277–1283.
[65] M. Roshani et al., Application of GMDH neural network technique to improve measuring precision of a simplified photon attenuation based two-phase flowmeter, Flow Measur. Instrum. 75 (2020).
[66] G.H. Roshani, S. Roshani, E. Nazemi, S. Roshani, Online measuring density of oil products in annular regime of gas-liquid two phase flows, Measurement 129 (2018) 296–301.
[67] G.H. Roshani, R. Hanus, A. Khazaei, M. Zych, E. Nazemi, V. Mosorov, Density and velocity determination for single-phase flow based on radiotracer technique and neural networks, Flow Meas. Instrum. 61 (2018) 9–14.
[68] G. Roshani, E. Nazemi, M. Roshani, Flow regime independent volume fraction estimation in three-phase flows using dual-energy broad beam technique and artificial neural network, Neural Comput. Appl. 28 (1) (2017) 1265–1274.
[69] G. Roshani, E. Nazemi, Intelligent densitometry of petroleum products in stratified regime of two phase flows using gamma ray and neural network, Flow Meas. Instrum. 58 (2017) 6–11.
[70] G.H. Roshani, E. Nazemi, M.M. Roshani, Intelligent recognition of gas-oil-water three-phase flow regime and determination of volume fraction using radial basis function, Flow Meas. Instrum. 54 (2017) 39–45.
[71] G.H. Roshani, E. Nazemi, S.A.H. Feghhi, Investigation of using 60Co source and one detector for determining the flow regime and void fraction in gas–liquid two-phase flows, Flow Meas. Instrum. 50 (2016) 73–79.
[72] P. Lalbakhsh, B. Zaeri, A. Lalbakhsh, M.N. Fesharaki, Antnet with reward-penalty reinforcement learning, in: 2010 2nd International Conference on Computational Intelligence, Communication Systems and Networks, 2010, pp. 17–21-17–21.
[73] P. Lalbakhsh, B. Zaeri, A. Lalbakhsh, An improved model of ant colony optimization using a novel pheromone update strategy, IEICE Trans. Inf. Syst. E96-D (11) (2013). pp. 2309–2318-2309–2318.

[74] B.M. Karambasti et al., Design methodology and multi-objective optimization of small-scale power-water production based on integration of Stirling engine and multi-effect evaporation desalination system, Desalination 526 (2022) 115542.
[75] L. Falkovsky, S. Pershoguba, Optical far-infrared properties of a graphene monolayer and multilayer, Phys. Rev. B 76 (15) (2007) 153410.
[76] F. Parandin, Ultra-compact terahertz all-optical logic comparator on GaAs photonic crystal platform, Opt. Laser Technol. 144 (2021) 107399.
[77] F. Parandin et al., Two-Dimensional photonic crystal Biosensors: A review, Opt. Laser Technol. 144 (2021) 107397.
[78] M. Abdollahi, F. Parandin, A novel structure for realization of an all-optical, one-bit half-adder based on 2D photonic crystals, J. Comput. Electron. 18 (4) (2019) 1416–1422.
[79] H. Saghaei, A. Zahedi, R. Karimzadeh, F. Parandin, Line defects on As2Se3-Chalcogenide photonic crystals for the design of all-optical power splitters and digital logic gates, Superlatt. Microstruct. 110 (2017) 133–138.
[80] M.M. Karkhanehchi, F. Parandin, A. Zahedi, Design of an all optical half-adder based on 2D photonic crystals, Photon Netw. Commun. 33 (2) (2017) 159–165.
[81] F. Parandin, M.-R. Malmir, M. Naseri, All-optical half-subtractor with low-time delay based on two-dimensional photonic crystals, Superlatt. Microstruct. 109 (2017) 437–441.
[82] F. Parandin, M.M. Karkhanehchi, Terahertz all-optical NOR and AND logic gates based on 2D photonic crystals, Superlatt. Microstruct. 101 (2017) 253–260.
[83] F. Parandin, N. Mahtabi, Design of an ultra-compact and high-contrast ratio all-optical NOR gate, Opt. Quant. Electron. 53 (12) (2021) 1–9.
[84] F. Parandin et al., Optical 1-bit comparator based on two-dimensional photonic crystals, Appl. Opt. 60 (8) (2021) 2275–2280.
[85] F. Parandin, R. Kamarian, M. Jomour, A novel design of all optical half-subtractor using a square lattice photonic crystals, Opt. Quant. Electron. 53 (2) (2021) 1–10.
[86] F. Parandin, M.M. Karkhanehchi, M. Naseri, A. Zahedi, Design of a high bitrate optical decoder based on photonic crystals, J. Comput. Electron. 17 (2) (2018) 830–836.
[87] S. Rayatzadeh, G. Moloudian, Design and fabrication of a miniaturized lowpass-bandpass diplexer with wide tuning range and high isolation, J. Electromagn. Waves Appl. 33 (14) (2019) 1874–1889.
[88] G. Moloudian, M. Dousti, A. Ebrahimi, Design and fabrication of a compact microstrip low-pass filter with ultra-wide stopband and sharp roll-off-rate, J. ElEctromagnEtic WavEs Appl. 32 (6) (2018) 713–725.
[89] S. Karimi-khorrami, G. Moloudian, Design and fabrication of a microstrip lowpass filter with wide tuning range as harmonic suppression with application in Wilkinson power divider, Analog Integr. Circ. Sig. Process 107 (1) (2021) 155–163.
[90] G. Moloudian, M. Dousti, Design and fabrication of a compact microstrip lowpass-bandpass diplexer with high isolation for telecommunication applications, Int. J. RF Microwave Comput. Aided Eng. 28 (5) (2018) e21248.
[91] G. Moloudian, M. Dousti, A. Ebrahimi, Design and fabrication of a tunable microstrip lowpass-bandpass diplexer for telecommunication applications, Microwave Opt. Technol. Lett. 60 (3) (2018) 754–759.
[92] A. Lalbakhsh, M.U. Afzal, K.P. Esselle, S.L. Smith, Low-Cost Non-Uniform Metallic Lattice for Rectifying Aperture Near-Field of Electromagnetic Bandgap Resonator Antennas, IEEE Trans. Antennas Propag. 68 (5) (2020) 3328–3335.
[93] G. Moloudian, S.R. Miri Rostami, T. Björninen, Modified Wilkinson power divider with harmonics suppression and compact size for GSM applications, Int. J. RF Microwave Comput. Aided Eng. 30 (7) (2020) e22209.
[94] S. Roshani, A compact microstrip low-pass filter with ultra wide stopband using compact microstrip resonant cells, Int. J. Microwave Wireless Technolog. 9 (5) (2017) 1023–1027.
[95] M. Lu, W. Li, E.R. Brown, Second-order bandpass terahertz filter achieved by multilayer complementary metamaterial structures, Opt. Lett. 36 (7) (2011) 1071–1073.
[96] D. Smith, D. Vier, T. Koschny, C. Soukoulis, Electromagnetic parameter retrieval from inhomogeneous metamaterials, Phys. Rev. E 71 (3) (2005) 036617.
[97] Z. Li, Y.J. Ding, "Terahertz broadband-stop filters, IEEE J. Select. Top. Quant. Electron. 19 (1) (2012). pp. 8500705-8500705.